Biomedicine & Pharmacotherapy 175 (2024) 116785

Contents lists available at ScienceDirect

Biomedicine & Pharmacotherapy

journal homepage: www.elsevier.com/locate/biopha

Monastrol suppresses invasion and metastasis in human colorectal cancer cells by targeting fascin independent of kinesin-Eg5 pathway

Begoña Alburquerque-González [a,1], Silvia Montoro-García [a,1], Ángel Bernabé-García [b], Manuel Bernabé-García [c], Priscila Campioni-Rodrigues [d,e], Alejandro Rodríguez-Martínez [f,g], Irene Luque [f], Tuula Salo [h,i,j,k,l], Alfonso Pérez-Garrido [g], Horacio Pérez-Sánchez [g], María Luisa Cayuela [c], Ginés Luengo-Gil [a,m], Enrico Luchinat [n,o], Fatima Postigo-Corrales [a], Tommaso Staderini [n], Francisco José Nicolás [b,2], Pablo Conesa-Zamora [a,m,*,2]

[a] Health Sciences Faculty, Universidad Católica de Murcia (UCAM), Guadalupe, Spain
[b] Regeneración, Oncología Molecular y TGF-β. IMIB-Arrixaca, Carretera Madrid-Cartagena, El Palmar 30120, Spain
[c] Research group "Telomerasa, Envejecimiento y Cáncer", CIBERER, Hospital Clínico Universitario Virgen de la Arrixaca, IMIB-Arrixaca, Murcia, Spain
[d] ECM and Hypoxia research unit, Faculty of Biochemistry and Molecular Medicine, University of Oulu, Aapistie 7C, FI-90014, Oulu, Finland
[e] Microelectronic Research Unit, Faculty of Information Technology and Electrical Engineering, University of Oulu, FI-90570, Oulu, Finland
[f] Department of Physical Chemistry, Institute of Biotechnology and Excellence Unit in Chemistry Applied to Biomedicine and Environment, School of Sciences, University of Granada, Granada 18071, Spain
[g] Structural Bioinformatics and High-Performance Computing (BIO-HPC) Research Group, Universidad Católica de Murcia (UCAM), Guadalupe, Spain
[h] Oral Medicine and Pathology, Research Unit of Population Health, University of Oulu, Finland
[i] Medical Research Center and Oulu University Hospital, Aapistie 3, Oulu FI-90220, Finland
[j] Department of Oral and Maxillofacial Diseases, University of Helsinki, Haartmaninkatu 8, Helsinki FI-0014, Finland
[k] Translational Immunology Research Program (TRIMM) and iCAN Digital Precision Cancer Medicine Flagship, University of Helsinki, Finland
[l] Department of Pathology, Helsinki University Hospital, Helsinki, Finland
[m] Pathology and Clinical Analysis Department, Group of Molecular Pathology and Pharmacogenetics, Instituto Murciano de Investigación Biosanitaria (IMIB), Hospital Universitario Santa Lucía, Cartagena, Spain
[n] CERM – Magnetic Resonance Center and Dipartimento di Chimica, Università degli Studi di Firenze, Via Luigi Sacconi 6, Sesto Fiorentino 50019, Italy
[o] Consorzio Interuniversitario Risonanze Magnetiche di Metallo Proteine – CIRMMP, Via Luigi Sacconi 6, Sesto Fiorentino 50019, Italy

ARTICLE INFO

Keywords:
Monastrol
Fascin
Cytoskeletal rearrangement
Actin
Colorectal cancer
Tubulin
Invasion

ABSTRACT

Rearrangement of the actin cytoskeleton is a prerequisite for carcinoma cells to develop cellular protrusions, which are required for migration, invasion, and metastasis. Fascin is a key protein involved in actin bundling and is expressed in aggressive and invasive carcinomas. Additionally, fascin appears to be involved in tubulin-binding and microtubule rearrangement. Pharmacophoric-based *in silico* screening was performed to identify compounds with better fascin inhibitory properties than migrastatin, a gold-standard fascin inhibitor. We hypothesized that monastrol displays anti-migratory and anti-invasive properties via fascin blocking in colorectal cancer cell lines. Biophysical (thermofluor and ligand titration followed by fluorescence spectroscopy), biochemical (NMR), and cellular assays (MTT, invasion of human tissue), as well as animal model studies (zebrafish invasion) were performed to characterize the inhibitory effect of monastrol on fascin activity. In silico analysis revealed that monastrol is a potential fascin-binding compound. Biophysical and biochemical assays demonstrated that monastrol binds to fascin and interferes with its actin-bundling activity. Cell culture studies, including a 3D human myoma disc model, showed that monastrol inhibited fascin-driven cytoplasmic protrusions as well as invasion. *In silico*, confocal microscopy, and immunoprecipitation assays demonstrated that monastrol disrupted fascin-tubulin interactions. These anti-invasive effects were confirmed *in vivo*. *In silico* confocal microscopy and immunoprecipitation assays were carried out to test whether monastrol disrupted the fascin-tubulin interaction. This study reports, for the first time, the *in vitro* and *in vivo* anti-invasive properties of monastrol in colorectal

* Corresponding author at: Health Sciences Faculty, Universidad Católica de Murcia (UCAM), Guadalupe, Spain.
E-mail address: pablo.conesa@carm.es (P. Conesa-Zamora).
[1] These authors contributed equally to this work.
[2] These authors contributed equally to this work and share their last authorship.

https://doi.org/10.1016/j.biopha.2024.116785
Received 11 February 2024; Received in revised form 6 May 2024; Accepted 17 May 2024
Available online 22 May 2024

tumor cells. The number and types of interactions suggest potential binding of monastrol across actin and tubulin sites on fascin, which could be valuable for the development of antitumor therapies.

1. Introduction

Remarkable progress has been made in recent years towards the understanding, prevention, and treatment of malignant tumors; however, metastatic cancer remains a leading cause of disease-related mortality [1]. The protein fascin (*FSCN1* gene) is an actin-binding protein that plays a role in the organization of actin filament parallel bundles and the formation of microspikes, membrane ruffles, and stress fibers. It is also important for the formation of a diverse set of cell protrusions, such as filopodia, cell motility and migration [2–6]. In 2013, a meta-analysis reported that fascin was associated with an increased risk of metastasis and mortality in several cancer types, including colorectal cancer [7]. In the same year, our group identified fascin as an overexpressed protein in serrated adenocarcinoma (SAC) [8], a histological subtype of colorectal carcinoma characterized by very poor prognosis [9] and a more active invasive front, as evidenced by a higher occurrence of tumor budding, cytoplasmic pseudofragments, and an infiltrative tumor growth pattern [10]. Given the higher expression of fascin in SAC, its active role in promoting an invasive phenotype, and its overexpression is associated with poor survival in a wide variety of cancer types, it was postulated as a target for the search and development of therapeutic compounds with anti-fascin properties [11]. Accordingly, migrastatin and its macroketone analogs, considered typical inhibitors of fascin, have been shown to decrease metastatic tumor cell migration, invasion, and tumor metastasis [4]. Other potential fascin inhibitors have been identified using bioinformatics methods, which are particularly useful for drug discovery, especially when the target protein is defined [12].

Antimitotic agents are widely recognized as highly potent pharmaceuticals for combating various tumor types [13]. A pivotal group of motor proteins crucial for mitosis, namely the kinesin family, has emerged as a novel target for chemotherapy, namely the kinesin family [14]. Monastrol, a small molecule that arrests cells in mitosis by inhibiting Eg5, a member of the kinesin-5 family [15] already defined as an anticancer drug, is a widely used inhibitor of microtubule polymerization [16]. Suppression of Eg5 activity results in the activation of the spindle checkpoint, leading to the arrest of mitotic cells at the G2/M phase, ultimately culminating in cell death. Apart from its role in actin bundling, fascin interacts with microtubules thus contributing to cell adhesion and migration [17]. Consequently, targeting fascin beyond actin-dependent mechanisms may have implications for the development of therapies for cancer. In the current study, experimental and *in vivo* approaches were combined to confirm the fascin-inhibitory activity of monastrol and its potential as an antimetastatic agent.

2. Methods

2.1. In-silico screening

Pharmacophoric *in silico* screening was performed using LigandScout (LS) to identify compounds with better fascin inhibitory properties than migrastatin [18]. A pharmacophoric model was created from the core of the migrastatin (MGS_CORE) structure using LS [19]. This model was screened against a subset of the DrugBank library (version 5.0; of 9591 compounds, including 2037 approved by the American FDA, 96 nutraceuticals, and 6000 experimental) after fine-tuning a high-performance computing (HPC) cluster of all related necessary programs from the LS suite [20].

2.2. Blind docking

The monastrol structure was obtained from the DrugBank library, identified by the DB004331 code as mol2 and PDBQT files. The protein structure used for the calculations was extracted from the X-ray crystal structure of the fascin and NP-G2–044 inhibitor complex (PDB ID: 6B0T) [18]. Maestro and Auto Dock Tools preprocessed both structures to prepare structures for blind docking, obtaining mol2 and PDBQT files, respectively. After obtaining fascin and monastrol structural models, blind docking calculations were carried out using the meta-screener tool (https://github.com/bio-hpc/metascreener) to determine the top interacting poses and the details of their interactions between DB004331 and the fascin protein structure. Two different docking programs were used to perform blind docking: AutoDock Vina2 [21] and LeadFinder3 [22]. Both methods were executed in a consensus manner for fascin model targets, with monastrol as the query on the computing server [21].

2.3. Molecular dynamics simulations

Once the results from the different poses by Blind Docking were obtained, we conducted Molecular Dynamics simulations at 100 ns on the same fascin structure 6B0T for the poses corresponding to the known binding sites (actin-binding site 1 and 2, tubulin-binding site) and the one with the best docking score in the blind docking.

For this purpose, we first generated the topology of the ligand for each pose using an automatic script that utilizes ACPYPE [23]. We followed the subsequent steps of the molecular dynamics simulations using GROMACS 2022.3 [24]. These simulations were launched on the Picasso server using a GPU (NVIDIA A100-SXM4–40 GB) and 4 GB of RAM. First, we created the protein topology using the gmx pdb2gmx command, specifying amber99sb as the force field. The simulation box was defined as the solvated and added ions. The next step was an energy minimization stage of 2000 ps. After that, a single NvT equilibration stage of 50,000 ps and five NpT equilibration stages of 50,000 ps each were carried out. Finally, the dynamics were run at 100 ns, and the final trajectory generated was extracted in different frames to compare the ligand stability and movement with respect to the binding pose.

2.4. Recombinant Fascin1 expression and purification

Recombinant WT fascin was expressed in a BL21-gold (DE3) *E. coli* strain transformed with the pGEX-6 P-2A plasmid encoding full-length human fascin (UniProt Q16658) fused at the N-terminus with glutathione-S-transferase (GST), followed by the human rhinovirus 3 C protease cleavage site, according to a previously reported protocol [25]. Cells were grown at 28 °C in HTMC medium containing 100 μg/mL ampicillin, previously inoculated with a preculture of transformed cells grown overnight at 30 °C in Terrific Broth. Protein expression was induced at Optical Density $(O.D)_{600}$ = 1.2 with 0.5 mM IPTG and incubated overnight at 20 °C. The cells were centrifuged at 4 °C, 5000× *g* for 15 min, resuspended in binding buffer (20 mM sodium phosphate buffer, 150 mM NaCl, 5 mM dithiothreitol, 1 mM EDTA, pH 7.3), lysed by ultrasonication in an ice bath at 70 % amplitude for 3 min (10 s ON and 30 s OFF), and centrifuged for 40 min at 4 °C and 6000 *g*. The supernatant was loaded at 5 mL/min in a 5 mL GSTrap FF (Cytiva) column pre-equilibrated with binding buffer and further washed with 10 CV of binding buffer and 10 CV of cleavage buffer (50 mM Tris-HCl, 150 mM NaCl, 1 mM EDTA, 1 mM dithiothreitol, pH 7.5). Proteolytic cleavage was performed on-column by loading a PreScission protease stock solution (Cytiva) diluted 1/20 (v/v) in cleavage buffer, according to the

manufacturer's protocol, and incubated at 4 °C for 4 h. Fascin was eluted with 3 CV of cleavage buffer (5 mL/min), concentrated with a centrifugal concentrator (MWCO 30 kDa) at 4000 × g, T < 20 °C, and quantified by absorption at 280 nm using a predicted molar extinction coefficient $\varepsilon_{280} = 68{,}465\ M^{-1}\ cm^{-1}$. Fascin mutant 1–2 (R100E, R109E, K247E) and mutant 1–4 (K22E, K43E, R398E) [26] affected the junctions between 1 and 2 β-trefoil and 1 and 4 β-trefoil domains of the FSCN gene, respectively, as previously described [26]. Constructs were synthesized by GenScript Biotech (Leiden, Netherlands) by site-directed mutagenesis on the pGEX-6 P-2A plasmid containing the sequence of GST-WT fascin, and were expressed using the same protocol described above. This plasmid was kindly provided by Dr. Sabine Windhorst from the University Medical Center, Hamburg-Eppendorf, Germany.

2.5. Thermofluor

Differential Scanning Fluorimetry (Thermofluor) assays in the presence of 2 μM fascin were performed using a Bio-Rad C1000 Touch Thermal Cycler CFX96 RT-PCR system in a 96-well format, as described in Supplementary Material S1. Three replicates per compound, together with six internal controls, containing only free protein in 10% DMSO, were included in 96-well plates. The PCR plates were covered, shaken, centrifuged, incubated for 2 min at 20 °C inside the RT-PCR machine, and heated from 20 °C to 100 °C at a scan rate of 1 °C/min. T_m values were measured as the minimum of the first derivative of the thermal unfolding profile. Average Tm values for unbound fascin were obtained for each internal filter (FAM, HEX and T-Red) as reference for the determination of the changes in Tm upon compound binding (T_m, FAM = 55.6 ± 0.5 ºC, T_m, HEX = 56.0 ± 0.0 ºC, T_m, Tred = 56.2 ± 0.6 ºC), where the error values correspond to the standard deviation for the seven replicas included in each plate as internal controls).

2.6. Fluorescence titration

Fluorescence titration experiments were performed using a Cary Eclipse spectrofluorometer (Varian, Inc.). A 14.7 μM fascin solution was titrated with monastrol by adding increasing volumes of concentrated solutions. Emission spectra were recorded between 307 and 500 nm at 25 °C in 10 % DMSO, 100 mM NaCl, and 20 mM HEPES, pH 7.4, with the excitation wavelength fixed at 280 nm. Additional information regarding this procedure is provided in Supplementary Material S1.

2.7. Ligand-observed nuclear magnetic resonance

The saturation transfer difference (STD) and Water-Logy (WL) Nuclear Magnetic Resonance (NMR) experiments were recorded at 298 K with a Bruker Avance NEO 700 MHz (Bruker) equipped with either a cryogenically cooled TCI probe or a room temperature TCI probe. A 50 mM stock solution of monastrol was prepared by dissolving the powder in d_6-DMSO. STD and WL spectra were recorded on samples containing 250 μM monastrol, either alone or in the presence of 5 μM fascin (either WT or mutant) in NMR buffer (phosphate buffered saline (PBS, Gibco), pH 7.4 + 10% D_2O). The final DMSO concentration in all the NMR samples was 0.5%. For each sample, a 1D ^1H reference NMR spectrum (zgesgp pulse program], STD, and WL experiments were recorded. STD spectra (stddiffesgp.3 pulse program [27] were acquired with 512 scans with on-resonance irradiation at 0 ppm and off-resonance irradiation at −40 ppm. A train of 40 Gaussian-shaped pulses of 50 ms each was used for a total saturation time of 2 s. The final STD spectra are obtained by subtracting the saturated spectrum from the reference spectrum. WL spectra (ephogsygpno.2 pulse program [28] were acquired with 1024 scans with a 7.5 ms selective 180° Gaussian shaped pulse at the water signal frequency and a CLEANEX spinlock time of 30 ms. For both the STD and WL, a spectral width of 16 ppm, a 2.0 s relaxation delay, 16,384 data points for acquisition, and 65,536 points for transformation were used. The spectra were processed with a 1 Hz exponential line broadening using the Bruker TopSpin software.

2.8. Transmission electron microscopy detection

Transmission electron microscopy (TEM) was performed as described by Jansen et al., 2011 [26]. Briefly, actin (21 μM) was polymerized according to the protocol from the Actin-Binding Protein BiochemKit™ Muscle Actin (Cytoskeleton Inc., Denver, CO, USA), and then incubated with human recombinant fascin (Hypermol, Bielefeld, Germany) (molar ratio 1:1) for 30 min at room temperature. Fascin was incubated for 2 h at RT with 0.1 % DMSO (control), 100 μM migrastatin, or 100 μM monastrol. The samples were directly adsorbed onto 200 mesh copper grids for 30 s, blotted to remove excess solution, washed twice with distilled water, negatively stained with 1 % (w/v) uranyl acetate for 30 s, blotted, and dried again. TEM analysis of actin filaments and fascin-actin bundles was performed using a PHILIPS TECNAI 12 transmission electron microscope (FEI, Osaka, Japan) at an accelerating voltage of 80 kV and a magnification of up to 135,000 ×. Images were captured using a coupled camera (MegaView III). The number of filaments per bundle was counted manually in 20 pictures/condition and statistically analyzed using (Mann–Whitney U test).

2.9. Cell culture

The cell lines (HCT-116 and DLD-1) were obtained from the American Type Culture Collection (ATCC, Rockville, MD) and cultured in high-glucose Dulbecco's Modified Eagle's medium (DMEM) containing 10 % heat-inactivated fetal bovine serum (FBS), 50 U/mL penicillin, and 50 μg/mL streptomycin (Sigma Aldrich Chemical Co., USA) in an atmosphere of 5 % CO_2 and 95 % humidified air at 37 °C. Subcultures were performed when 90 % confluence was obtained.

2.10. Cell viability, proliferation and apoptosis assays

Exponentially growing cells were plated in triplicate in flat-bottomed 96-well plates (Nunc, Roskilde, Denmark) at 1500 cells/well. The next day, drugs were added in serial dilutions from 0.5 to 300 μM. The control wells contained medium without the drug plus 0.1 % DMSO. The plates were incubated for 72 h in a humidified 5% CO_2 incubator and assayed for cell viability. Tetrazolium (MTT) dissolved in phosphate-buffered saline (PBS); pH 7.2, at 1.9 mg/mL was added to the cells (30 μL/well). After incubation at 37 °C for 4 h, the medium was aspirated. The formazan crystals were dissolved in 200 μL DMSO for 30 min and the absorbance was read at 570 nm using a microtiter plate reader. The results were calculated as follows: cell viability (%) = average O.D. of wells/average O.D. of control wells. The MTT assay measures metabolic activity as an indicator of cell proliferation and viability. Since monastrol blocks mitosis, cell growth was quantified by flow cytometry (FCM) (Supplementary Materials).

2.11. Immunofluorescence

For immunofluorescence, round coverslips (Thermo Fisher, Waltham, MA, USA) were seeded with HCT-116 cells in the presence of 10% FBS. After cells reached 100% confluence, the serum-supplemented medium was removed and replaced with fresh serum-free medium for 24 h. Artificial wounding was performed by transversally dragging a sterilized razor blade on the central area of the coverslips. The coverslips were then placed in 6-well plates with 2 mL serum-free DMEM: control condition (0.1 % DMSO), 100 μM migrastatin, or 100 μM monastrol for 24 h. Cells were then fixed with Bouin (for fascin protein) or 4 % formaldehyde, permeabilized in 0.3% Triton X-100/PBS solution, and exposed to blocking buffer for 30 min. Samples were incubated for 1 h with an anti-fascin antibody (1/250) (55 K-2 clone; Santa Cruz Biotechnology, Heidelberg, Germany) in a wet chamber. Samples were

examined, and representative images were taken using a confocal microscope (LSM 510 META, ZEISS, Jena, Germany). Additional information is provided in the Supplementary Material S1.

2.12. Colocalization assay

To test the colocalization of fascin and β-tubulin, an immunofluorescence assay was performed as previously described [26,29]. The following commercial antibodies were used: mouse anti-β-tubulin (DSHB#E7) and anti-fascin ([EP5902] (ab126772)). Images were acquired using a Confocal Leica SP8 microscope. Colocalization analyses were performed using the JaCoP plugin colocalization module of the Fiji ImageJ software [30].

2.13. Transwell invasion assay

The invasive capacities of HCT-116 cells and their inhibitory effects were determined using Cytoselect TM 24 Well Cell Invasion Assay (Basement Membrane Colorimetric Format) with coated Transwell chambers (8 μm pore size). The number of invaded cells was determined using an inverted phase contrast microscope and quantified using a spectrophotometer at λ=560 nm. Likewise, the invasive cells were counted and analyzed using ImageJ v1.52p software (National Institute of Health, Bethesda, MD, USA). Each experiment was performed in triplicate (Supplementary Material S1).

2.14. Myoma organotypic invasion model

To improve the reliability of the experimental model compared with the real tumor microenvironment, cancer cell invasion was assessed in myoma organotypic cultures and performed according to a previously published myoma model protocol [31,32]. Briefly, uterine leiomyoma tissues were obtained by routine surgery after obtaining written informed consent from the donors, and their use was approved by The Ethics Committee of the Oulu University Hospital. The myoma tissue was sliced into 5 mm pieces, and disks were made with an 8-mm biopsy punch (Kai Industries Co., Gifu, Japan). Myoma disks were pre-incubated in control conditions (0.1 % DMSO), 100 μM migrastatin, or 100 μM monastrol at 4 °C for 48 h. The myoma disks were placed into Transwell inserts (diameter 6.5 mm; Corning Incorporated, Corning, NY) and 700,000 cells in 50 μL of media were added on top of each myoma disk. The cells were allowed to attach overnight, and the myoma disks were transferred onto uncoated nylon disks resting on curved steel grids in 12-well plates with 1 mL of medium plus compounds in each well. Human cells were left to invade the myoma disks for 14 days, while changing the treatment media every 3 days. Additional information is provided in the Supplementary Material S1. ImageJ v1.46o software (National Institute of Health, Bethesda, MD, USA) was used to measure the invasion area and depth. Each experiment was performed in triplicates.

2.15. Zebrafish invasion and metastasis assays

Colonization of zebrafish (*Danio rerio*) embryos by human cancer cells was performed as previously described [33]. Briefly, colorectal cancer cells were trypsinized, washed, and stained with fluorescent CM-Dil (Vibrant, Invitrogen) according to the manufacturer's instructions. 50–100 labeled cells were injected into the yolk sac of dechorionated zebrafish embryos. Embryos were treated with control conditions (0.1 % DMSO), 100 μM migrastatin, or 100 μM monastrol. Fish with fluorescently labeled cells appearing outside the implantation area at 2 h post-injection were excluded from further analysis. All other fish were incubated at 35 °C for 48 h and analyzed using a SteReoLumar V12 stereomicroscope equipped with an AxioCam MR5 camera (Carl Zeiss). The evaluation criterion for embryos colonized by human cancer cells was the presence of more than three cells outside the yolk sac. The zebrafish colonization index was calculated as the proportion of embryos colonized in the wild type and mutant cells divided by the proportion of invaded embryos in the pcDNA transfected cells.

The metastasis assay was based on a previous study by Fior et al., in which a metastatic potential assay on zebrafish was performed [34]. Native HCT-116 cells were stained and xenografted as previously described. From the 3rd day post-injection, larvae were fed with ZEBRAFEED by Sparos (<100 μm), and the treatments were changed daily. On the 6th day post-injection, the larvae were examined for tumor growth and invasion using a fluorescent microscope. The metastatic potential of human cancer cells was evaluated by the presence of cell colonies (dividing cells) outside the yolk sac. The experiments were repeated in triplicate, obtaining an average value at 4 days post-xenograft (invasion assay) and 6 days post-xenograft (metastasis assay). All the protocols in the manuscript comply with the recommendation, the approval of which was obtained from the participating institutions, and in accordance with the ethical standards laid down in the 1964 Declaration of Helsinki and its later amendments. The extended treatment with migrastatin in the metastatic assay (beyond the 4th day) was toxic to the larvae; therefore, only monastrol results were presented.

2.16. Immunoprecipitation and western blot

For immunoprecipitation (IP), we followed the protocol described in Section [35]. Briefly, cells were stimulated and total protein extracts were obtained by lysis of harvested cells using lysis buffer: 50 mM HEPES pH 7.2, 150 mM NaCl, 1 mM EDTA, 1.2 mM $MgCl_2$, 1 % Triton X-100, 10 % Glycerol (all from Sigma-Aldrich, St Louis, MO, USA), supplemented with 1 mM DTT, 25 mM NaF, 25 mM β-glycerophosphate, 1:100 phosphatase inhibitors (I and II) and 1:100 protease inhibitors (all from Sigma-Aldrich, St Louis, MO, USA). The cells were treated with 0.1 % DMSO and 100 μM monastrol. Samples of the extract taken prior to IP were processed in parallel with the immunoprecipitates and were considered as inputs. For IP, 500 ng of control IgG and ß-tubulin antibody was added to 400 μg of total protein extract and incubated for 1 h at 4 °C. Antibodies were purified using A and G protein 4 Fast Flow coupled Sepharose (Cytiva, Uppsala, Sweden) previously blocked with BSA 0.2 mg/mL (SantaCruz Biotechnology, Heidelberg, Germany) in lysis buffer. Samples were washed with supplemented lysis buffer, and the resin was resuspended in 60 μL of loading buffer. Samples were then analyzed by SDS-PAGE, followed by western blotting (WB) with recombinant 1:2000 anti-fascin antibody (2 h, 5% milk) and 1:250 anti--β-tubulins (2 h, 1 % BSA). Secondary antibodies used were anti-rabbit IgG horseradish peroxidase linked F(ab')2 I fragment from donkey (GE Healthcare, Little Chalfont, United Kingdom) and horseradish peroxidase-conjugated rat anti-mouse IgG1 (Beckton Dickinson, Franklin Lakes, NJ, USA). WBs were visualized using horseradish peroxidase substrate (ECL; GE Healthcare, Little Chalfont, United Kingdom). Images were obtained using ChemiDoc XRS® (Bio-Rad, Hercules, CA, USA).

2.17. Data analysis

Data are expressed as means ± standard deviation (SD). Data were analyzed for statistical differences using Student's t-test for paired and unpaired data after testing for normal distribution of the data. For the *in vitro* experiments, the Kruskal-Wallis (KW) test was performed for comparisons between groups. Differences were considered significant at an error probability of $p < 0.05$. SPSS 22.0 software was used for the rest of the statistical analyses (SPSS, Inc., Chicago, Illinois, USA).

3. Results

3.1. In-silico screening

After *in silico* screening calculations and careful visual inspection of the results, monastrol was selected as one of the top 31 candidates for experimental validation. The pharmacophoric model and 3D alignment derived for migrastatin are depicted in Supplementary Material S1. When Blind Docking calculations were completed, a consensus of the results of AutoDock Vina and LeadFinder Docking calculations was carried out. Thus, we obtained the best-scoring DB004331 clustered poses of the ligand from the results of the two techniques, sorted by binding energy score and the interactions of these poses with fascin residues via PLIP [36]. Finally, we obtained a protein-ligand complex snapshot using the PyMOL program [37]. We have indicated the actin-binding sites, microtubule-binding sites, and clustered poses with interactions at these sites. First, the clustered poses in the two known actin sites 1,6 are found in the top positions of the calculations. In Autodock Vina blind docking results (Fig. 1A), poses 2 (Score: −6.11 kJ/mol) and 3 (Score: −5.72 kJ/mol) correspond with the known actin-binding sites. In the case of the Lead Finder method (Fig. 1B), the first and second clustered poses also interact with the two indicated actin-binding sites with scores of −8.51 kJ/mol and −7.30 kJ/mol, respectively. Both calculations revealed interactions between monastrol and the key residues Leu40 for actin-binding site 1 and Phe216 for actin-binding site 2. In addition, in results obtained by both methods, the interactions between monastrol and residues that are part of the tubulin-binding site sequence can be observed (Supplementary material S2A) [17]. The results of Autodock Vina showed hydrogen bond interactions in Lys244 and Ala245 residues in the clustered pose 17 (Score: −4.48 kJ/mol) (Supplementary material S2A).

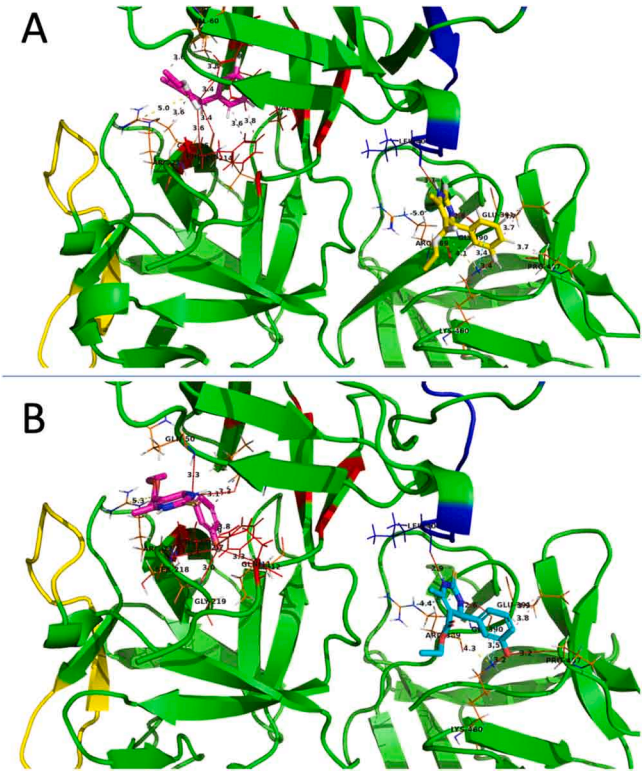

Fig. 1. Interactions between the monastrol compound and fascin actin-binding site 1 (blue) and 2 (red). (A) Interactions obtained from AutoDock Vina calculations. (B) Interactions obtained from Lead Finder calculations. Red dashed lines indicate hydrogen bond interactions and dashed pink lines indicate hydrophobic interactions.

On the other hand, we found a clustered pose in rank 13 (Score: −6.11 kJ/mol) in Lead Finder calculations (Supplementary material S2B), where we observed hydrophobic interactions with Lys244 and hydrogen bond formation with Lys244, Ala245, and Lys247. Finally, after performing the consensus analysis, the generated poses with ranks 1 and 2 corresponded to actin-binding sites 1 and 2, respectively, showing interactions between monastrol and Leu40 in actin-binding site 1 (Supplementary material S3), and between residues Phe216 and Gln11 in actin-binding site 2. Regarding the tubulin-binding site, three poses with interactions with some of its sequence residues can be observed (Supplementary material S3) in ranks 13, 25, and 31, respectively, with monastrol interacting with the following residues: Ala242, Lys 244, Ala245, and Lys247, all of which belong to the amino acid sequence that describes the tubulin-binding site. The results obtained from Blind Docking indicate that monastrol can bind with equal probability to both the actin-binding sites and the tubulin-interacting site. The number and types of interactions suggest potential binding across these sites on fascin.

Finally, the results obtained from the MD simulations showed that the ligand pose was more stable during the simulation time. The ligand remained in the specific binding site in the two cases of the binding sites 1 and 2. In addition, they did not shift to another possible binding pocket during the simulation and maintained the same conformation as the initial one.

3.2. Ligand-based NMR assays

The binding of monastrol to fascin was confirmed using ligand-based NMR spectroscopy (Fig. 2). WaterLOGSY (WL) [28] and saturation transfer difference (STD) [27] experiments were performed to assess the ligand–protein interactions in solution. WL exploits magnetization transfer from the solvent to the bound ligand, leading to the buildup of signals with negative signs, whereas STD exploits saturation transfer from the protein to the bound ligand, leading to the buildup of signals with positive signs in the difference spectrum. Both methods are sensitive to low-to-medium affinity ligands and have been previously applied to screen compounds that bind to fascin [25]. Both WL and STD confirmed that monastrol interacted with fascin (Fig. 2). In the WL spectrum, the signals of monastrol were clearly attenuated in the presence of fascin, but there was no sign inversion (Fig. 2A), whereas very weak signals were observed in the STD spectrum (Fig. 2B), suggesting that monastrol directly interacts with fascin, albeit weakly. The interaction of monastrol with the two fascin mutants was also investigated. In these previously described mutants [26], positively charged residues involved in the interaction with actin were mutated at the interface between domains 1 and 2 (mutant 1–2) and between domains 1 and 4 (mutant 1–4). WL and STD NMR spectra showed that monastrol interacted with mutant 1–4 with similar strength to WT fascin, whereas the interaction with mutant 1–2 was more apparent (Supplementary material S4). The fact that mutant 1–2 affects the binding affinity of monastrol suggests that the interaction takes place close to that region, which is consistent with binding to actin-binding site 2.

3.3. Thermofluor and fluorescence titration

The direct interaction between the compounds selected by virtual screening and fascin was examined *in vitro* using a differential fluorescence screening (Thermofluor) assay, as described before [25,38]. The results of DFS assay are summarized in Table 1.

Some compounds resulted in distorted thermal unfolding profiles, from which reliable T_m values could not be extracted, probably due to compound interference with the Sypro fluorescence signal. Other induced a clear shift in T_m to higher values, indicative of a binding-induced stabilization of the protein. Among those that could be analyzed, imipramine had been tested in our previous work [38]. Monastrol (compound 28) induced an increase in Tm of approximately

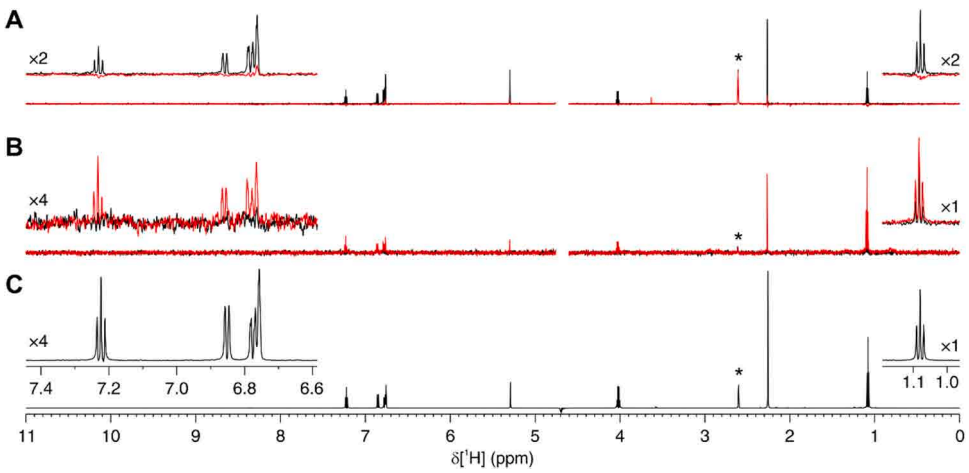

Fig. 2. Interaction between monastrol and fascin determined by ligand-based NMR spectroscopy. (A) WL NMR spectra of 250 μM monastrol alone (black) and in combination with 5 μM fascin (red). (B) STD NMR spectra of samples. (C) reference 1 H NMR spectrum of monastrol. The insets show the aromatic (left) and methyl (right) signals. The 1 H signal from d_6-DMSO is marked with an asterisk.

Table 1
Thermal shift assay results.

Compound	T_m, FAM (°C)	ΔT_m, FAM (°C)	T_m, HEX (°C)	ΔT_m, HEX (°C)	T_m, TRed (°C)	ΔT_m, TRed (°C)
Free fascin	55.7 ± 0.5	-	56.0 ± 0,0	-	56.2 ± 0.6	-
Monastrol, 100 μM	57.7 ± 0,6	2.0 ± 1.1	57.7 ± 0.6	1.7 ± 0.6	58.0 ± 0.0	1.8 ± 0.6

2 °C, suggesting specific binding to fascin (Fig. 3). The binding of monastrol to fascin was validated *in vitro* using fluorescence titration experiments, rendering a dissociation constant in the high μM range (K_D = 183 μM).

3.4. Monastrol significantly decreased the fascin-induced actin bundles

Negative contrast in TEM allowed visualization of actin fibers formed in the presence of fascin and comparison of the effects of inhibitors. Under control conditions, actin-fascin consisted of a highly densely packed actin bundle (Fig. 4 A and B). When fascin was pre-incubated with either 100 μM migrastatin or monastrol separately, disorganization of the bundles was observed, resulting in fewer filaments than in the control (Kruskal–Wallis test, $p<0.001$) (Fig. 4 C-E, respectively). No statistically significant difference was observed between the two inhibitors.

3.5. Monastrol compromises colorectal cell line proliferation but not viability, and affects actin rearrangement in lamellipodia

According to the data presented in Supplementary Material S5, the working concentration of monastrol was set to 100 μM for subsequent *in vitro* studies. The effect of monastrol on the reorganization of the actin cytoskeleton, which includes the protrusion of the lamellipodium at the cell front and filopodia formation, was assessed by immunofluorescence (Fig. 5). Prominent filopodia lamellipodium formation was observed under control conditions, whereas these cytoskeleton structures were absent in cells treated with both inhibitors (Fig. 5). Assays with HaCaT cells in the presence of monastrol as well as with Epidermal Growth Factor (EGF) and migration inhibitor targeting Mek pathway (PD98059) were also performed in parallel, as in previous studies (data not shown) [25,38,39]. The lamellipodia protrusion number was calculated under different conditions and was significantly lower after inhibitor treatments (Supplementary Table S1).

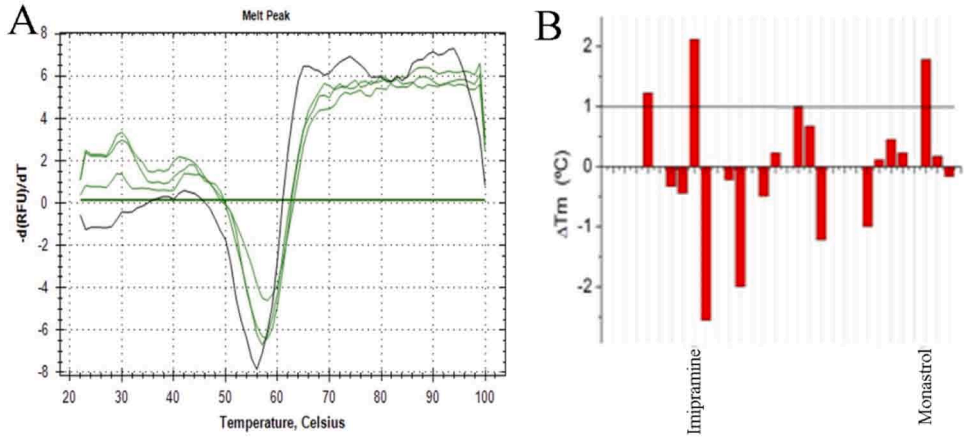

Fig. 3. Differential fluorescence screening (Thermofluor) assay suggested specific binding of monastrol to fascin. (A) First derivative of the differential scanning fluorometry profile for fascin (black line) and fascin in the presence of monastrol 100 μM (fascin concentration, 2 μM; 10% DMSO). (B) Changes in denaturation temperature, established as the minimum in the first derivative of the thermal denaturation profile, induced by the presence of different compounds.

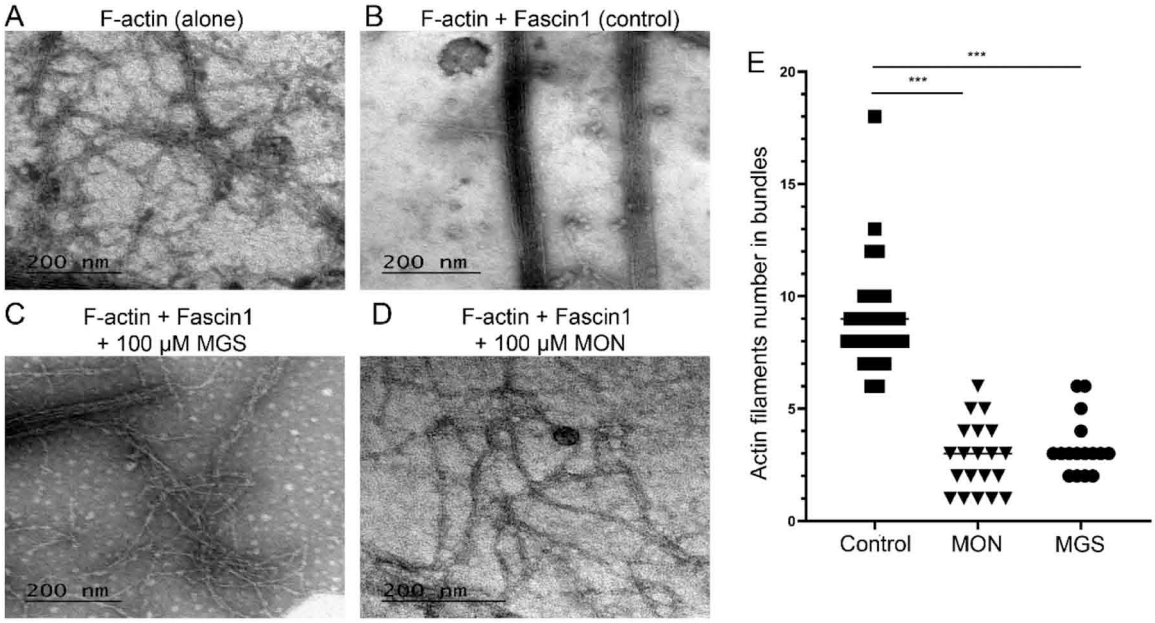

Fig. 4. Monastrol interferes with the formation of actin bundles, as evidenced by TEM (A) actin bundle formation alone, (B) actin bundle formation in the presence of fascin (C) MGS: migrastatin, and (D) MON: monastrol. (E) Quantitative analysis of the number of actin filaments in several images acquired by TEM (n=3, *** $p < 0.001$, Kruskal-Wallis test).

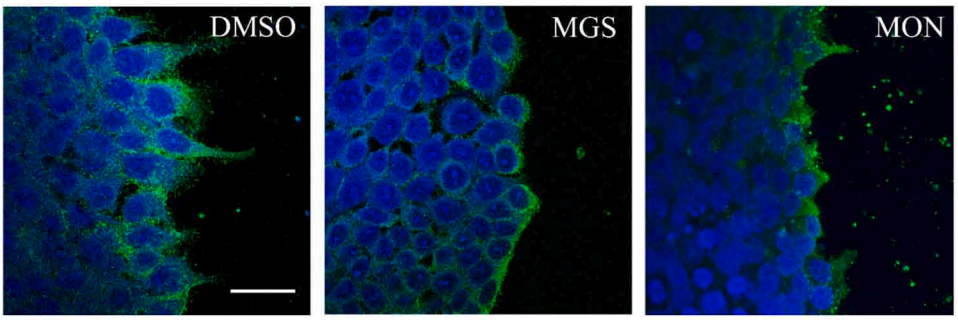

Fig. 5. Monastrol interferes with cytoplasmic protrusions at the migrating edge in a wound scratch assay of HCT-116 cells. Wounded cells were treated with DMSO (control), MGS (migrastatin 100 µM), or MON (monastrol 100 µM). Fascin is shown in green and nuclei in blue. Scale barr 24 µm.

3.6. Monastrol inhibits cell invasion of colorectal cancer cells

Tumor cell invasion involves the acquisition of migration properties and the ability to degrade the extracellular matrix (ECM) [40]. Therefore, we performed a Transwell assay on Matrigel, which resembles the ECM basement membrane composition. Similar to migrastatin, monastrol inhibited tumor cell migration in HCT-116 cells (all $p<0.01$) (Supplementary material S6) [38]. As already shown in our previous studies, an interesting *in vitro* model for the assay of the anti-invasive properties of potential inhibitors is the human uterine myoma tissue-derived myoma disc model [41]. Fig. 6 shows that 100 µM monastrol was an effective inhibitor in this model in a dose-dependent manner, which was comparable to that of migrastatin (all $p<0.001$).

3.7. Monastrol reduces invasion and metastasis in zebrafish larvae model

Consistent with our previous studies [25,38], the *in vivo* anti-invasive potential of monastrol was tested using a well-established zebrafish larval xenograft invasion model. As shown in Fig. 7A, significant inhibition of DLD-1 and HCT-116 cell invasion was observed in larvae grown in the presence of both 100 µM migrastatin and 100 µM monastrol when compared to control conditions (all $p<0.05$). DLD-1 cells showed lower invasion ability than HCT-116 cells (Fig. 7A). Due to the higher efficacy of inhibitors in HCT-116 cells, a metastasis model (up to 6th day post-injection) was established with these cancer cells (Fig. 7C). Monastrol was found to inhibit the formation of metastatic foci in HCT-116 cells in the same zebrafish model ($p<0.0001$, Fig. 7D).

3.8. Monastrol disrupts Fascin-tubulin interaction

Since monastrol has been described as an inhibitor of Eg5, a member of the kinesin-5 family [42,43], an IP assay was carried out to test whether the β-tubulin-fascin interaction could be affected in the presence of this compound. Monastrol treatment for 24 h decreased the fascin/β-tubulin interaction (Fig. 8). Moreover, a colocalization study using immunofluorescence for both proteins in HCT-116 cells showed a reduction in colocalization of both proteins in the presence of monastrol 100 µM. The calculation of the Pearson correlation coefficient showed a significant decrease in the colocalization of both proteins in the presence of 100 µM monastrol when compared to the control conditions (0.1 % DMSO) (Supplementary material S7).

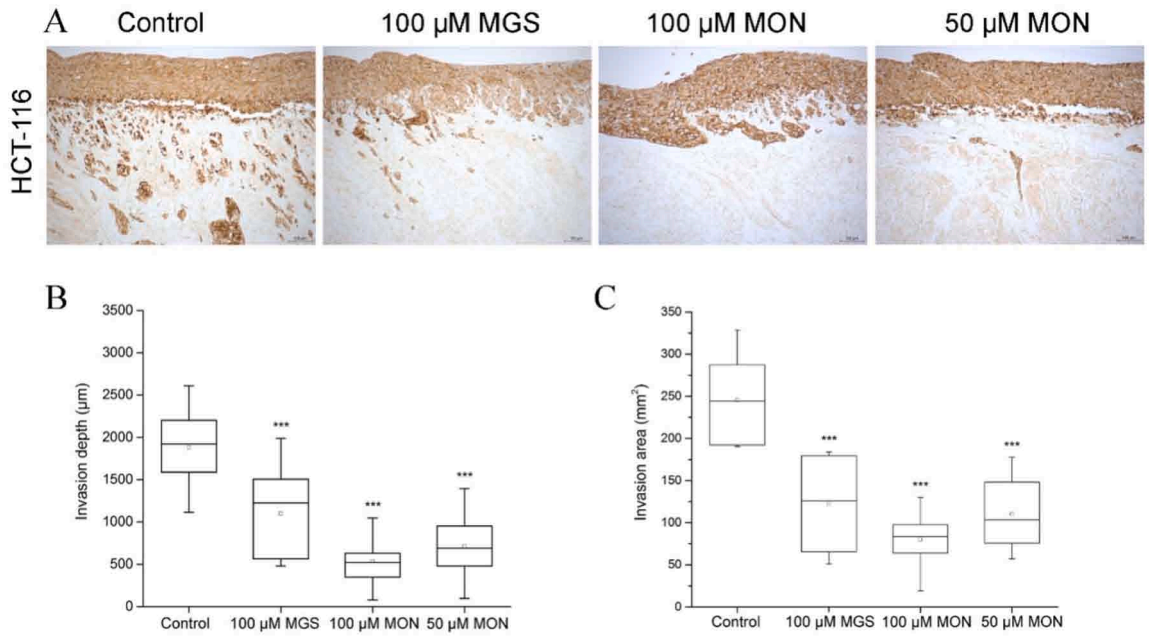

Fig. 6. Monastrol prevents the invasion of HCT-116 cells in an organotypic myoma invasion model. (A) Immunohistochemical staining demonstrating the effect of 50 and 100 μM monastrol (MON) and 100 μM migrastatin (MGS) on invasion, compared to the control in HCT-116 colorectal cancer cells. Box plots showing the quantification of (B) depth and (C) area of invasion of HCT-116 cells. The mean ± SD are illustrated in the graphs (n = 3; *** $p<0.001$, Kruskal-Wallis test).

4. Discussion

Metastasis is the cause of > 90 % of cancer deaths [44]. This process is driven by intricate rearrangement of the actin cytoskeleton, which allows tumor cells to acquire the ability to migrate and invade surrounding tissues by forming specialized cellular structures, such as lamellipodia and invapodia [45]. Fascin protein plays a pivotal role in the formation of these structures because of its unique ability to bundle actin filaments together [46]. Interestingly, fascin expression is strongly associated with highly metastatic cancers with poor prognosis, particularly in those with advanced-stage disease, which has acquired the properties of migration and invasion [47]. However, the actin bundling activity is just one of the fascin contributions to tumor development and promotion as other non-canonical fascin functions are being discovered including chemoresistance, immune evasion, metabolic reprogramming, and tubulin cytoskeleton rearrangement [17,46,48–52]. These findings, along with the virtually absent expression of fascin in normal epithelia and its overexpression in aggressive cancers such as SAC and triple-negative breast cancer (TNBC), which have no molecular targeted therapy available, make the discovery of fascin inhibitors a crucial task.

With this aim, we performed a pharmacophoric in silico screening of more than 9500 compounds from the DrugBank library, which yielded monastrol, an allosteric mitotic kinesin Eg5 inhibitor involved in microtubule (MT) rearrangement, as a potential fascin blocker. The result was not surprising; Villari et al. previously demonstrated the effect of fascin on MT dynamics, reporting that fascin amino acids 234–250 are involved in direct MT binding and that this effect is essential for focal adhesion assembly of breast cancer cells [17]. In 2016, Marques et al. showed that monastrol has greater antiproliferative activity in human adenocarcinoma cells than in non-tumor breast cells [53]. Riahi et al. in 2019 [54], in a molecular docking study, indicated that monastrol has structural similarity to nifedipine, which, in a previous fascin bioassay using *Drosophila* neurons [55], proved to be a fascin inhibitor. Accordingly, monastrol and migrastatin core structures were placed in a common spatial position required for actin-binding activity. First, regarding actin-binding site 1, the residue with more interactions close to the actin-binding site was Leu40 [18], appearing in both docking algorithms and showing a hydrophobic union. Other critical residues, such as Ser39 and Lys43, were found in at least one docking technique. In addition, we identified interactions associated with actin-binding site 2, including Phe216 and Gln11 [6]. Such ligand protein interactions were also further related to the fascin thermal denaturation profiles in the presence of monastrol, which showed a T_m shift with a similar magnitude as the previously reported fascin inhibitor imipramine [38].

Monastrol is a racemate comprising equimolar amounts of R- and S-monastrol and is a novel, low-molecular-weight molecule with multiple potential therapeutic roles. It has been identified as an antineoplastic, urease inhibitor, antileishmanial, and antimitotic agent [15]. Although many reports have been devoted to elucidating the mechanism of action of monastrol as a mitotic inhibitor in the cell cycle, few examples of anticancer activity have been reported [56]. The primary objective of this study was to investigate the potential of monastrol as an inhibitor of Fascin in colorectal cancer cells. To establish its efficacy, inhibition by monastrol was compared to that of migrastatin, a well-known fascin inhibitor used as a control, in both *in vitro* and *in vivo* assays.

Despite previous suggestions of monastrol's potential as a fascin inhibitor, it has not been thoroughly characterized until this study [54]. The interaction of monastrol with fascin was validated *in vitro* by a Thermal Shift assay, fluorescence titration, NMR spectroscopy, and TEM. Overall, the *in vitro* data indicate that monastrol directly interacts with fascin with an affinity in the high-μM range, although such approaches cannot be directly extrapolated to more complex physiological conditions or to current biological effects. To choose colorectal cell lines with different endogenous fascin expression, RT-qPCR on RNA extracted from eight cell lines was performed in our previous work [38]; thus, DLD-1 and HCT-116 were selected as cell lines as examples of low and high fascin expression, respectively. In cell culture experiments, monastrol effectively reduced fascin-driven cellular protrusions in colorectal cancer cells.

This inhibitory effect on lamellipodia formation resulted in decreased cell invasion, mirroring the effect of the fascin inhibitor migrastatin. Furthermore, the findings were extended to a 3D human organotypic model designed to mimic the tumor microenvironment. In this model, monastrol was found to decrease both the depth and area of

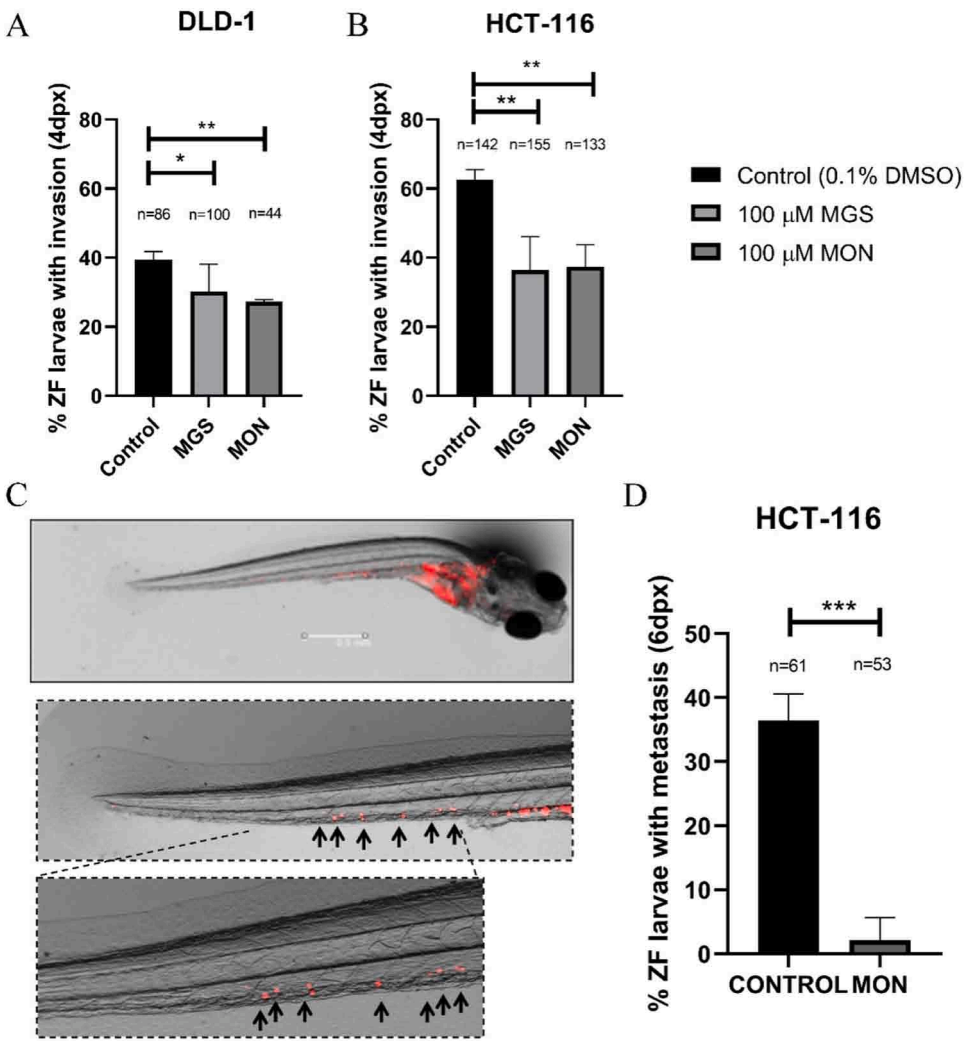

Fig. 7. Anti-invasive and antimetastatic potential of monastrol in zebrafish xenotransplantation model. At four days post-xenographt, the invasive cells (A) DLD-1 and (B) HCT-116) were counted in the presence of 100 μM migrastatin and 100 μM monastrol. (C) Six days post-injection, the larvae were examined to evaluate the micro-metastasis developed by invading native HCT-116 cells. (D) HCT-116 cell growth outside the yolk sac in the presence of 100 μM monastrol. MGS, migrastatin; MON, monastrol. Data are shown as mean ± SD; compared with the control condition, * $p<0.05$, 0.01** $p = 0.001–0.009$, *** $p = 0.0001–0.0009$.

invasion by HCT-116 colorectal cancer cells in a dose-dependent manner, similar to the effects observed with migrastatin. Overall, this study highlights the potential of monastrol as a promising candidate for inhibiting fascin and reducing cancer invasion, particularly in colorectal cancer, shedding light on a novel therapeutic approach to combat this disease.

In the *in vivo* model, we observed that monastrol induced a decrease in invasion and formation of metastatic foci in colorectal cancer cells. Indeed, the drug effect was more pronounced in HCT-116 cells than in DLD-1 cells, and this difference may be related to the varying fascin levels in these cell lines. Nevertheless, additional studies in different animal models are necessary to confirm the effectiveness of monastrol as an agent that inhibits cancer cell migration and invasion. Given recent research indicating that fascin interacts with tubulin [52] and that monastrol is considered an inhibitor of MT dynamics [15], we performed Blind Docking calculations to explore potential interaction sites on the entire surface of the fascin protein (see Supplementary material S4). Our data suggest that monastrol could potentially interact with both the actin-binding sites 1 and 2 of fascin, as well as the fascin-tubulin binding site. These interaction areas aligned with previously reported interaction sites based on mutagenesis studies [17]. To further validate these *in silico* findings, we conducted IP and confocal immunofluorescence assays to investigate whether monastrol could disrupt the binding between fascin and tubulin. In the absence of the inhibitor, the recovery of tubulin and fascin was higher in the pellets, indicating a strong association. Interestingly, the Pearson correlation coefficient also revealed the colocalization of both proteins in lamellipodia, although this colocalization was reduced in the presence of monastrol. Overall, the number and types of interactions suggest potential binding between fascin, tubulin, and actin. Consequently, these synergistic binding actions could reduce the functionality of the C protein and impede cell migration.

Our findings suggest that monastrol holds promise as a drug worth exploring in preclinical studies. This could be a valuable candidate for clinical trials aimed at preventing metastatic processes in patients with primary colorectal cancer who test positive for fascin expression. Furthermore, the potential benefits of monastrol could extend to other cancer types characterized by high fascin expression, such as TNBC, as suggested by Brandl et al. (2015 [57]. These results may also have an impact on the function of fascin in chemoresistance, as monastrol treatment may reverse this phenomenon and work synergistically with chemotherapeutic agents that target MT, such as taxanes or vinca alkaloids.

This study, for the first time, sheds light on the anti-migratory and anti-invasive properties of monastrol in colorectal tumor cells, possibly due, but not restricted to, the direct inhibition of fascin. In addition, our

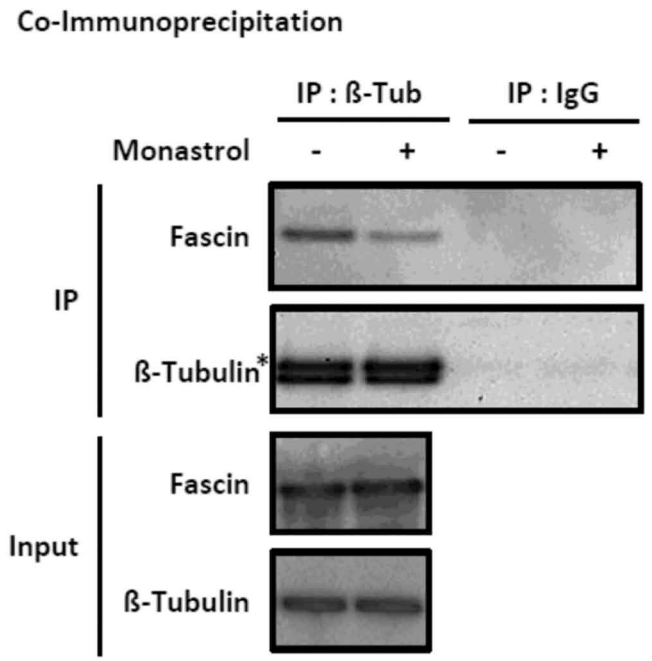

Fig. 8.. Monastrol interferes with fascin and β-tubulin interaction. The cells were treated with DMSO (control) or 100 μM monastrol for 24 h. β-tubulin was purified by immunoprecipitation. Fascin and β-tubulin were detected using western blotting. IP: immunoprecipitation. β-Tub: β-Tubulin. The upper band (*) represents the cross-reaction of the secondary antibody to IgG.

data demonstrated that monastrol interacts outside the actin-binding site, which should be explored further. These results implied that monastrol has clinical potential as a promising therapy for the treatment of invasive and metastatic cancers, offering new avenues for combating the spread of these diseases.

Ethics declarations

The Authors declare no Competing Financial or Non-Financial Interests.

Author information

These authors contributed equally and share first authorship: Begoña Alburquerque-González and Silvia Montoro-García. These authors contributed equally to this work and share the last authorship: Francisco José Nicolás and Pablo Conesa-Zamora.

CRediT authorship contribution statement

Alejandro Rodríguez-Martínez: Investigation. **Pablo Conesa-Zamora:** Writing – review & editing, Writing – original draft, Visualization, Validation, Supervision, Software, Resources, Project administration, Methodology, Investigation, Funding acquisition, Formal analysis, Data curation, Conceptualization. **Francisco José Nicolás:** Writing – original draft, Supervision, Methodology, Investigation, Formal analysis. **Tuula Salo:** Investigation. **Irene Luque:** Investigation. **Ángel Bernabé-García:** Methodology, Investigation. **Fatima Postigo Corrales:** Investigation. **Begoña Alburquerque-González:** Writing – review & editing, Writing – original draft, Visualization, Validation, Resources, Methodology, Formal analysis, Data curation, Conceptualization. **Enrico Luchinat:** Investigation. **Priscila Campioni-Rodrigues:** Investigation. **Manuel Bernabé-García:** Methodology, Investigation. **Tommaso Staderini:** Investigation. **Horacio Pérez-Sánchez:** Software, Resources, Investigation, Data curation. **Alfonso Pérez-Garrido Pérez-Garrido:** Investigation. **Silvia Montoro-García:** Writing – review & editing, Writing – original draft, Validation, Software, Resources, Methodology, Investigation, Formal analysis, Data curation, Conceptualization. **Ginés Luengo-Gil:** Writing – review & editing, Validation, Methodology, Investigation. **María Luisa Cayuela:** Investigation.

Declaration of Competing Interest

I would like to disclose that none of the co-authors have financial or non-financial conflicts of interest that could influence the objectivity, integrity, or validity of the research presented in this manuscript. We do not have any financial affiliations, direct or indirect, with any commercial entities or organizations that may have a direct interest in the subject matter or materials discussed in the article.

Our sole commitment is to the advancement of scientific knowledge and the dissemination of accurate and unbiased research findings.

Thank you for your attention to this matter. If you require any further information or clarification, please do not hesitate to contact me.

Data Availability

The data generated and/or analyzed in the current study are available from the corresponding author upon reasonable request.

All data generated or analyzed in this study are included in this published article.

Acknowledgments

This work was supported by two funds (Refs: PI15/00626 and PI18/00144) from the Instituto de Salud Carlos III (Ministry for Science and Innovation). GLG holds a grant from the Spanish Society of Hematology and Hemotherapy (*Beca de Investigación* FEHH/Janssen, 2021–2023). The authors acknowledge Dr. Sabine Windhorst from the University Medical Center Hamburg-Eppendorf, Germany for kindly providing the mutant plasmids.

Appendix A. Supporting information

Supplementary data associated with this article can be found in the online version at doi:10.1016/j.biopha.2024.116785.

References

[1] J. Budczies, et al., The landscape of metastatic progression patterns across major human cancers, Oncotarget 6 (2015) 570–583, https://doi.org/10.18632/oncotarget.2677.
[2] M. Conacci-Sorrell, C. Ngouenet, S. Anderson, T. Brabletz, R.N. Eisenman, Stress-induced cleavage of Myc promotes cancer cell survival, Genes Dev. 28 (2014) 689–707, https://doi.org/10.1101/gad.231894.113.
[3] S.H. Kim, et al., Frequent expression of follicular dendritic cell markers in Hodgkin lymphoma and anaplastic large cell lymphoma, J. Clin. Pathol. 66 (2013) 589–596, https://doi.org/10.1136/jclinpath-2012-201425.
[4] L. Chen, S. Yang, J. Jakoncic, J.J. Zhang, X.Y. Huang, Migrastatin analogues target fascin to block tumour metastasis, Nature 464 (2010) 1062–1066, https://doi.org/10.1038/nature08978.
[5] N. Kotzor, M. Lechmann, E. Zinser, A. Steinkasserer, The soluble form of CD83 dramatically changes the cytoskeleton of dendritic cells, Immunobiology 209 (2004) 129–140, https://doi.org/10.1016/j.imbio.2004.04.003.
[6] S. Yang, et al., Molecular mechanism of fascin function in filopodial formation, J. Biol. Chem. 288 (2013) 274–284, https://doi.org/10.1074/jbc.M112.427971.
[7] V.Y. Tan, S.J. Lewis, J.C. Adams, R.M. Martin, Association of fascin-1 with mortality, disease progression and metastasis in carcinomas: a systematic review and meta-analysis, BMC Med. 11 (2013) 52, https://doi.org/10.1186/1741-7015-11-52.
[8] P. Conesa-Zamora, et al., Expression profiling shows differential molecular pathways and provides potential new diagnostic biomarkers for colorectal serrated adenocarcinoma, Int. J. Cancer 132 (2013) 297–307, https://doi.org/10.1002/ijc.27674.
[9] J. Garcia-Solano, et al., Clinicopathologic study of 85 colorectal serrated adenocarcinomas: further insights into the full recognition of a new subset of colorectal carcinoma, Hum. Pathol. 41 (2010) 1359–1368, https://doi.org/10.1016/j.humpath.2010.04.002.
[10] J. Garcia-Solano, P. Conesa-Zamora, J. Trujillo-Santos, M.J. Makinen, M. Perez-Guillermo, Tumour budding and other prognostic pathological features at invasive

margins in serrated colorectal adenocarcinoma: a comparative study with conventional carcinoma, Histopathology 59 (2011) 1046–1056, https://doi.org/10.1111/j.1365-2559.2011.04043.x.
[11] H. Liu, et al., Fascin actin-bundling protein 1 in human cancer: promising biomarker or therapeutic target? Mol. Ther. Oncol. 20 (2021) 240–264, https://doi.org/10.1016/j.omto.2020.12.014.
[12] X. Xia, Bioinformatics and drug discovery, Curr. Top. Med. Chem. 17 (2017) 1709–1726, https://doi.org/10.2174/1568026617666161116143440.
[13] R.J. van Vuuren, M.H. Visagie, A.E. Theron, A.M. Joubert, Antimitotic drugs in the treatment of cancer, Cancer Chemother. Pharmacol. 76 (2015) 1101–1112, https://doi.org/10.1007/s00280-015-2903-8.
[14] S.M. Myers, I. Collins, Recent findings and future directions for interpolar mitotic kinesin inhibitors in cancer therapy, Future Med. Chem. 8 (2016) 463–489, https://doi.org/10.4155/fmc.16.5.
[15] J.C. Cochran, J.E. Gatial 3rd, T.M. Kapoor, S.P. Gilbert, Monastrol inhibition of the mitotic kinesin Eg5, J. Biol. Chem. 280 (2005) 12658–12667, https://doi.org/10.1074/jbc.M413140200.
[16] Z. Maliga, T.M. Kapoor, T.J. Mitchison, Evidence that monastrol is an allosteric inhibitor of the mitotic kinesin Eg5, Chem. Biol. 9 (2002) 989–996, https://doi.org/10.1016/s1074-5521(02)00212-0.
[17] G. Villari, et al., A direct interaction between fascin and microtubules contributes to adhesion dynamics and cell migration, J. Cell Sci. 128 (2015) 4601–4614, https://doi.org/10.1242/jcs.175760.
[18] J. Huang, et al., Structural insights into the induced-fit inhibition of fascin by a small-molecule inhibitor, J. Mol. Biol. 430 (2018) 1324–1335, https://doi.org/10.1016/j.jmb.2018.03.009.
[19] H. Geppert, M. Vogt, J. Bajorath, Current trends in ligand-based virtual screening: molecular representations, data mining methods, new application areas, and performance evaluation, J. Chem. Inf. Model. 50 (2010) 205–216, https://doi.org/10.1021/ci900419k.
[20] G. Wolber, T. Langer, LigandScout: 3-D pharmacophores derived from protein-bound ligands and their use as virtual screening filters, J. Chem. Inf. Model. 45 (2005) 160–169, https://doi.org/10.1021/ci049885e.
[21] O. Trott, A.J. Olson, AutoDock Vina: improving the speed and accuracy of docking with a new scoring function, efficient optimization, and multithreading, J. Comput. Chem. 31 (2010) 455–461, https://doi.org/10.1002/jcc.21334.
[22] O.V. Stroganov, F.N. Novikov, V.S. Stroylov, V. Kulkov, G.G. Chilov, Lead finder: an approach to improve accuracy of protein-ligand docking, binding energy estimation, and virtual screening, J. Chem. Inf. Model. 48 (2008) 2371–2385, https://doi.org/10.1021/ci800166p.
[23] A. Bernardi, R. Faller, D. Reith, K.N. Kirschner, ACPYPE update for nonuniform 1–4 scale factors: conversion of the GLYCAM06 force field from AMBER to GROMACS, SoftwareX 10 (2019) 100241, https://doi.org/10.1016/j.softx.2019.100241.
[24] M.J. Abraham, et al., GROMACS: High performance molecular simulations through multi-level parallelism from laptops to supercomputers, SoftwareX 1-2 (2015) 19–25, https://doi.org/10.1016/j.softx.2015.06.001.
[25] B. Alburquerque-Gonzalez, et al., The FDA-approved antiviral raltegravir inhibits fascin1-dependent invasion of colorectal tumor cells in vitro and in vivo, Cancers 13 (2021), https://doi.org/10.3390/cancers13040861.
[26] S. Jansen, et al., Mechanism of actin filament bundling by fascin, J. Biol. Chem. 286 (2011) 30087–30096, https://doi.org/10.1074/jbc.M111.251439.
[27] M. Mayer, B. Meyer, Characterization of ligand binding by saturation transfer difference NMR spectroscopy, Angew. Chem. Int Ed. Engl. 38 (1999) 1784–1788, https://doi.org/10.1002/(SICI)1521-3773(19990614)38:12<1784::AID-ANIE1784>3.0.CO;2-Q.
[28] C. Dalvit, G. Fogliatto, A. Stewart, M. Veronesi, B. Stockman, WaterLOGSY as a method for primary NMR screening: practical aspects and range of applicability, J. Biomol. NMR 21 (2001) 349–359, https://doi.org/10.1023/a:1013302231549.
[29] A. Alcaraz, et al., Amniotic membrane modifies the genetic program induced by TGFss, stimulating keratinocyte proliferation and migration in chronic wounds. PLOS One 10 (2015) e0135324 https://doi.org/10.1371/journal.pone.0135324.
[30] J. Schindelin, et al., Fiji: an open-source platform for biological-image analysis, Nat. Methods 9 (2012) 676–682, https://doi.org/10.1038/nmeth.2019.
[31] T. Salo, et al., Organotypic three-dimensional assays based on human leiomyoma-derived matrices, Philos. Trans. R. Soc. Lond. B Biol. Sci. 373 (2018), https://doi.org/10.1098/rstb.2016.0482.
[32] P. Astrom, R. Heljasvaara, P. Nyberg, A. Al-Samadi, T. Salo, Human tumor tissue-based 3D in vitro invasion assays, Methods Mol. Biol. 1731 (2018) 213–221, https://doi.org/10.1007/978-1-4939-7595-2_19.
[33] B. Jelassi, et al., P2X(7) receptor activation enhances SK3 channels- and cystein cathepsin-dependent cancer cells invasiveness. Oncogene 30 (2011) 2108–2122, https://doi.org/10.1038/onc.2010.593.
[34] R. Fior, et al., Single-cell functional and chemosensitive profiling of combinatorial colorectal therapy in zebrafish xenografts, Proc. Natl. Acad. Sci. USA 114 (2017) E8234–E8243, https://doi.org/10.1073/pnas.1618389114.
[35] E.M. Garcia-Vizcaino, S. Liarte, J.L. Alonso-Romero, F.J. Nicolas, Sirt1 interaction with active Smad2 modulates transforming growth factor-beta regulated transcription. Cell Commun. Signal. 15 (2017) 50, https://doi.org/10.1186/s12964-017-0205-y.
[36] S. Salentin, S. Schreiber, V.J. Haupt, M.F. Adasme, M. Schroeder, PLIP: fully automated protein-ligand interaction profiler, Nucleic Acids Res. 43 (2015) W443–447, https://doi.org/10.1093/nar/gkv315.
[37] R.E. Rigsby, A.B. Parker, Using the PyMOL application to reinforce visual understanding of protein structure, Biochem Mol. Biol. Educ. 44 (2016) 433–437, https://doi.org/10.1002/bmb.20966.
[38] B. Alburquerque-Gonzalez, et al., New role of the antidepressant imipramine as a Fascin1 inhibitor in colorectal cancer cells, Exp. Mol. Med. 52 (2020) 281–292, https://doi.org/10.1038/s12276-020-0389-x.
[39] S. Montoro-Garcia, et al., Novel anti-invasive properties of a Fascin1 inhibitor on colorectal cancer cells, J. Mol. Med. 98 (2020) 383–394, https://doi.org/10.1007/s00109-020-01877-z.
[40] T. Han, et al., How does cancer cell metabolism affect tumor migration and invasion? Cell Adhes. Migr. 7 (2013) 395–403, https://doi.org/10.4161/cam.26345.
[41] S. Nurmenniemi, et al., A novel organotypic model mimics the tumor microenvironment, Am. J. Pathol. 175 (2009) 1281–1291, https://doi.org/10.2353/ajpath.2009.081110.
[42] T.U. Mayer, et al., Small molecule inhibitor of mitotic spindle bipolarity identified in a phenotype-based screen, Science 286 (1999) 971–974, https://doi.org/10.1126/science.286.5441.971.
[43] J. Aseervatham, Cytoskeletal remodeling in cancer, Biology 9 (2020), https://doi.org/10.3390/biology9110385.
[44] C.L. Chaffer, R.A. Weinberg, A perspective on cancer cell metastasis, Science 331 (2011) 1559–1564, https://doi.org/10.1126/science.1203543.
[45] E. Sarantelli, A. Mourkakis, L.C. Zacharia, A. Stylianou, V. Gkretsi, Fascin-1 in cancer cell metastasis: old target-new insights, Int. J. Mol. Sci. 24 (2023), https://doi.org/10.3390/ijms241411253.
[46] M.C. Lamb, T.L. Tootle, Fascin in cell migration: more than an actin bundling protein, Biology 9 (2020), https://doi.org/10.3390/biology9110403.
[47] K.W. Min, et al., Fascin expression predicts an aggressive clinical course in patients with advanced breast cancer, Oncol. Lett. 10 (2015) 121–130, https://doi.org/10.3892/ol.2015.3191.
[48] Y. Wang, et al., Fascin inhibitor increases intratumoral dendritic cell activation and anti-cancer immunity, Cell Rep. 35 (2021) 108948, https://doi.org/10.1016/j.celrep.2021.108948.
[49] Y. Wu, et al., LYAR promotes colorectal cancer progression by upregulating FSCN1 expression and fatty acid metabolism, Oxid. Med. Cell Longev. 2021 (2021) 9979707, https://doi.org/10.1155/2021/9979707.
[50] S. Lin, et al., Fascin promotes lung cancer growth and metastasis by enhancing glycolysis and PFKFB3 expression, Cancer Lett. 518 (2021) 230–242, https://doi.org/10.1016/j.canlet.2021.07.025.
[51] H. Ghebeh, et al., Fascin is involved in the chemotherapeutic resistance of breast cancer cells predominantly via the PI3K/Akt pathway, Br. J. Cancer 111 (2014) 1552–1561, https://doi.org/10.1038/bjc.2014.453.
[52] L.S. Heinz, et al., Strong fascin expression promotes metastasis independent of its F-actin bundling activity, Oncotarget 8 (2017) 110077–110091, https://doi.org/10.18632/oncotarget.22249.
[53] L.A. Marques, et al., Antiproliferative activity of monastrol in human adenocarcinoma (MCF-7) and non-tumor (HB4a) breast cells, Naunyn Schmiede Arch. Pharm. 389 (2016) 1279–1288, https://doi.org/10.1007/s00210-016-1292-9.
[54] N. Riahi, et al., Design, Synthesis and molecular docking studies of some tetrahydropyrimidine derivatives as possible fascin inhibitors, Chem. Biodivers. 16 (2019) e1800339, https://doi.org/10.1002/cbdv.201800339.
[55] R. Kraft, et al., A cell-based fascin bioassay identifies compounds with potential anti-metastasis or cognition-enhancing functions, Dis. Model Mech. 6 (2013) 217–235, https://doi.org/10.1242/dmm.008243.
[56] D. Russowsky, et al., Synthesis and differential antiproliferative activity of Biginelli compounds against cancer cell lines: monastrol, oxo-monastrol and oxygenated analogues, Bioorg. Chem. 34 (2006) 173–182, https://doi.org/10.1016/j.bioorg.2006.04.003.
[57] M.B. Brandl, et al., Computational analysis of image-based drug profiling predicts synergistic drug combinations: applications in triple-negative breast cancer, Mol. Oncol. 8 (2014) 1548–1560, https://doi.org/10.1016/j.molonc.2014.06.007.